Geophys. J. Int. (2004) **158,** 744–752 doi: 10.1111/j.1365-246X.2004.02308.x

D-Rex, a program for calculation of seismic anisotropy due to crystal lattice preferred orientation in the convective upper mantle

Édouard Kaminski, Neil M. Ribe and Jules T. Browaeys

Laboratoire de Dynamique des Systèmes Géologiques - IPG Paris and Université Paris 7 *Denis Diderot,* 4 *place Jussieu,* 75252 *Paris cédex* 05, *France*

Accepted 2004 March 25. Received 2004 March 25; in original form 2003 August 8

SUMMARY

Models of development of lattice preferred orientation (LPO) of crystals aggregates in convective flow are necessary to interpret the anisotropic seismic signature of the Earth's upper mantle. For that purpose we previously developed a model of LPO evolution in olivine aggregates by plastic deformation and dynamic recrystallization by subgrain rotation and grain-boundary migration. This paper presents a refined version of that model, called D-Rex (for dynamic recrystallization-induced LPO), a public version of which is made available on our web site. The code displays two new features: (1) enstatite is incorporated in the aggregates and (2) grain-boundary sliding (GBS) of small grains is taken into account. Enstatite is incorporated on the assumption of no direct interaction with olivine. The fast (*a*-)axis of enstatite grains tend to be parallel to the slow (*c*-)axis of olivine, which dilutes the total anisotropy. Grain boundary sliding is included using a threshold dimensionless volume fraction χ, defined as the ratio of the initial size of the grains over the size for which GBS is the dominant mechanism of deformation. Grains with a dimensionless volume smaller than χ do not rotate by plastic deformation and their strain energy is set to zero. Comparison with torsion experiments at very large strain constrains the threshold dimensionless volume to 0.3 ± 0.1. The incorporation of grain-boundary sliding prevents the LPO from becoming singular at large strains and yields more realistic predictions. Our kinematic formalism and the model's semi-analytical character insures that it is fast, robust and stable. It can be applied efficiently to arbitrary 3-D convective flows.

Key words: dynamic recrystallization, LPO, mantle convection, seismic anisotropy.

1 INTRODUCTION

Seismic anisotropy in the upper mantle is routinely attributed to the lattice-preferred orientation (LPO) of olivine crystals in the convective flow (Nicolas & Christensen 1987). Experimental deformations of olivine crystals show that the change of the crystallographic orientation of the crystals is due to dislocation creep and to dynamic recrystallization by subgrain rotation and grain-boundary migration (Nicolas *et al.* 1973; Zhang *et al.* 2000; Bystricky *et al.* 2000; Lee *et al.* 2002). These observations can be used to elaborate theoretical models of LPO development by plastic deformation and dynamic recrystallization.

To develop a model of LPO evolution, one can start from the atomic level to predict the behaviour of the crystal defects and the resulting LPO. Such an approach is useful for better understanding of the microphysics of the deformation process but is very difficult to implement in a macroscopic convection code. An alternative is to use a rather simple model that accounts for the basic macrophysics of the deformation mechanisms and is easy to incorporate in convection codes (Chastel *et al.* 1993; Tommasi 1998; Dawson & Wenk 2000; Blackman *et al.* 2002; Becker *et al.* 2003). Here we propose such a simplified theory for crystal rotation by plastic deformation and dynamic recrystallization, involving only a small number of parameters constrained by comparison with laboratory experiments.

Models of plastic deformation calculate the deformation of the different crystals forming the aggregate as a function of their orientation relative to an imposed stress tensor (Etchecopar 1977; Takeshita *et al.* 1990; Ribe & Yu 1991; Wenk *et al.* 1991; Chastel *et al.* 1993; Tommasi *et al.* 2000). In models of dynamic recrystallization, the deformation of each crystal is used to estimate its density of dislocations which itself drives dynamic recrystallization (Wenk & Tomé 1999; Kaminski & Ribe 2001). Grains favourably oriented for the deformation (soft grains) tend to have a large density of dislocations and nucleate new subgrains by subgrain rotation. The dislocation-free subgrains lower the plastic energy of the soft grains and make them grow by grain-boundary migration. As a result, soft orientations dominate the LPO as observed in laboratory experiments (Nicolas *et al.* 1973; Zhang & Karato 1995; Bystricky *et al.* 2000).

Models of dynamic recrystallization of olivine are in very good agreement with the LPO displayed by the relict grains in simple shear experiments for strain up to 200 per cent (Wenk & Tomé

1999; Kaminski & Ribe 2001). In the most recent detailed experimental study of Lee *et al.* (2002), two families of grains have been described: the largest population is formed by soft grains with a high density of dislocations, whereas a secondary population is formed by grains with a small density of dislocations (see their Figs 2 and 3). These two families are the ones favoured by grain boundary migration and dominate the LPO in Kaminski & Ribe (2001). Furthermore, the model of Kaminski & Ribe (2001) has recently been used successfully to predict new LPO observed in deformed wet olivine aggregates (Jung & Karato 2001; Kaminski 2002). One may also note that the underlying assumption of Kaminski & Ribe (2001), that global strain compatibility can be relaxed when dynamic recrystallization occurred, is confirmed by the observations of Lee *et al.* (2002) that diffusion creep and grain-boundary sliding—the two mechanisms that can relax global strain compatibility—are enhanced by dynamic recrystallization.

At larger strains, however, the models tend to generate a very strong LPO with a very sharp single peak orientation, and the aggregate behaves like a single crystal, which is obviously not very realistic (Blackman *et al.* 2002). In fact, torsion experiments indicate that for strains up to 500 per cent the LPO does not become singular and may even still display a secondary peak (Bystricky *et al.* 2000). The anisotropy predicted by the available models is thus probably too large. Furthermore, the anisotropy of an olivine single crystal is larger than the anisotropy of an enstatite single crystal (Weidner *et al.* 1978). In the mantle, there is probably about 30 per cent of enstatite (in addition to garnet and clinopyroxene) (Dick *et al.* 1984), which will decrease the total anisotropy of the aggregates. To account for these shortcomings in the new version of the model, we incorporate enstatite as in Ribe (1992) and we include a parametrization of grain-boundary sliding.

2 PHENOMENOLOGY OF DYNAMIC RECRYSTALLIZATION

Dynamic recrystallization is a rather complex process that is still not completely understood. However, the basic physics underlying the process seems to be established firmly enough to propose first-order models. Plastic deformation of a crystal in an aggregate occurs by dislocation creep on slip systems. Each dislocation creates a local stress field which builds up the global strain energy of the crystal. Dynamic recrystallization tends to decrease the strain energy by two processes: grain-boundary migration and nucleation (Poirier & Guillopé 1979; Karato 1987). The difference of strain energy drives grain-boundary migration from low-energy grains to high-energy grains. Moreover, high strain energy (i.e. high dislocation density) triggers nucleation of new strain-free grains, notably by subgrain rotation. The resulting bulk energy of the grain is reduced and the grain may grow by grain-boundary migration.

Dynamic recrystallization may induce large variations of size among the grains forming the aggregates if grain-boundary migration is intense. Because deformation mechanisms are also a function of the size of the grains, dynamic recrystallization may activate different deformation mechanisms in the same aggregate: large grains deform dominantly by dislocation creep, whereas small grains deform dominantly by grain-boundary sliding or even diffusion creep (Karato *et al.* 1986). As a consequence, the LPO displayed by small grains—generated by dynamic recrystallization—is predicted to be more dispersed, as observed by Lee *et al.* (2002) (see their Fig. 3). The calculation of the contribution of the small grains to the aggregate LPO requires a quantitative treatment of grain-boundary sliding in the model.

3 FORMULATION OF THE MODEL

We consider an aggregate of N crystals of volume fraction f_ν, ($\nu = 1, 2, \ldots, N$). The orientation of each grain relative to an external or 'laboratory' frame is described by a set of three Eulerian angles $g_\nu = (\phi_1^\nu, \theta^\nu, \phi_2^\nu)$ and the related matrix of direction cosines, a_{ij}^ν. The quantity a_{ij}^ν is the cosine of the angle between the ith crystal axis ($i = 1, 2, 3$ for the axes [100], [010] and [001] respectively) and the jth external axis. Before deformation, the volume fraction of the grains is set to $1/N$ and their orientation is random. As a function of the externally imposed deformation, the large grains deform by an intracrystalline slip, which controls the rotation of the crystallographic axes, and undergo dynamic recrystallization, which controls the evolution of the volume fractions. The small grains deform by grain-boundary sliding.

The model is based on an 'averaged field' formalism. We do not keep track of the exact interaction between one grain and its neighbours but each grain is considered as an inclusion in a homogeneous isotropic medium whose properties are the weighted average of the properties of all grains as in the other usual models (Tommasi *et al.* 2000). The grain shape is assumed to be spherical due to dynamic recrystallization.

As in the original formulation of Ribe & Yu (1991), the present model is only kinematic and does not introduce the macroscopic stress explicitly. All the equations in the following will be made dimensionless using a strain rate scale $\dot{\epsilon}_o$. In particular the results will be presented as a function of dimensionless time, $\dot{\epsilon}_o t$. In pure shear, this dimensionless time is equal to half the natural strain $\ln(c_1/c_3)$, with c_1 the long axis of the finite strain ellipsoid and c_3 its short axis. In simple shear, the natural strain is $\ln(a/c) = 2\sinh^{-1}(\dot{\epsilon}_o t)$.

3.1 Plastic deformation

In Kaminski & Ribe (2001)'s model, as in Ribe & Yu (1991), individual grains of each mineral phase m in the aggregate respond to an imposed deformation by a combination of a rigid body rotation and simple shear on s independent slip systems ($s = 1, 2, 3$ for olivine and $s = 1$ for enstatite), each of which is assumed to obey a power-law rheology with an activation stress τ_m^s and a stress exponent n (in the following, n is set to 3.5 for olivine and enstatite Bai *et al.* 1991). The deformation rate of each crystal ν is described by a local velocity gradient tensor

$$d_{ij}^\nu = G_{ij}^\nu \gamma^\nu - \varepsilon_{ijk}\omega_k^\nu, \tag{1}$$

where ω^ν is the rotation rate of the crystallographic axes and γ^ν is the rate of slip on the weakest slip system. Here and henceforth, the Einstein summation convention is assumed for all indices, except ν and s. The tensor G_{ij}^ν is equivalent to a Schmid tensor, and is given by (Ribe & Yu 1991)

$$G_{ij}^\nu = 2\sum_{s=1}^{S} \beta_m^{s\nu} l_i^{s\nu} n_j^{s\nu}, \tag{2}$$

where $l_i^{s\nu}$ and $n_j^{s\nu}$ are unit vectors in the slip direction and normal to the slip plane of slip system s, respectively, and

$$\beta_m^{s\nu} = \frac{\tau_o I^{s\nu}}{\tau_m^s I^{1\nu}} \left| \frac{\tau_o I^{s\nu}}{\tau_m^s I^{1\nu}} \right|^{n-1}, \tag{3}$$

Table 1. Reference dimensionless resolved shear stresses.

Mineral	(010) [100]	(001) [100]	(010) [001]	(100) [001]
Olivine (dry)	1	2	3	∞
Olivine (wet—high stress)	3	2	1	∞
Olivine (wet—low stress)	3	2	∞	1
Enstatite	∞	∞	∞	1

Experimental data from deformation experiments on single crystals (Raleigh *et al.* 1971; Kohlstedt & Goetze 1974; Durham & Goetze 1977; Bai *et al.* 1991; Hanson & Spetzler 1994; Jin *et al.* 1994). The wet conditions are obtained by comparison between experiments and numerical predictions (Jung & Karato 2001; Kaminski 2002). The symbol ∞ indicates an inactive shear plane.

where $I^{sv} = l_i^{sv} n_j^{sv} E_{ij}$, with E_{ij} the imposed macroscopic strain rate tensor, and τ_o is a reference activation stress chosen among the slip systems of the different mineral phases forming the aggregate. In the following, we will choose the activation stress for the softest slip system of olivine as a reference. If the mineral phase in question has only one slip system, (3) simplifies to

$$\beta_m^v = \left(\frac{\tau_o}{\tau_m^1}\right)^n. \tag{4}$$

The factor β_m^{sv} gives the relative activities of the different slip systems of the different mineral phases as a function of their critical reference shear stresses and of their orientations relative to the macroscopic strain rate tensor. Because the reference stress τ_o is the same for all the phases in the aggregate, β quantifies the relative deformation of the phases. A phase with very large activation stresses (small β) will hardly deform while a softer phase (β close to 1) will accommodate the imposed deformation.

For a given externally imposed velocity gradient tensor D_{ij} the plastic deformation of the crystals is only a function of their orientation and of the values of the dimensionless reference resolved shear stresses (RRSS) τ_m^s/τ_o for the shear planes of the different phases. The values of the RRSS are obtained from laboratory measurements on single crystals and are given in Table 1. The effect of water can be incorporated at that stage by changing accordingly the values of the RRSS (Kaminski 2002). The quantities γ^v, ω_i^v, are then analytically calculated by minimizing the difference between the local crystal velocity gradient tensor d_{ij}^v and the imposed global velocity gradient tensor D_{ij} (Kaminski & Ribe 2001). Von Mises' criterion states that five independent slip systems are required for a crystal to follow an arbitrary imposed deformation. As olivine has only three independent slip systems, the local and imposed velocity gradient tensors are not equal in general. An extra deformation of the grains (of about 10 per cent (Kaminski & Ribe 2001)), by dislocation climb and/or grain-boundary sliding, is thus implicitly required in the model. From ω_i^v, one can calculate the change of orientations of the crystals, whereas γ^v is used to estimate strain energy.

3.2 Strain energy

The stored strain energy of a grain is a function of its dislocation density. It has been observed that the dislocation density in deforming olivine crystals reaches a steady state at a small strain (about 1 per cent (Durham *et al.* 1977)). At steady state and in the absence of nucleation, the stored strain energy density E of a crystal would be just the strain energy stored by the dislocations,

$$E = A\rho\mu b^2, \tag{5}$$

with A a dimensionless constant, μ the shear modulus and b is the length of the Burgers' vector. In a highly deformed grain, the dislocations can rearrange to form dislocation walls and nucleate new grains. These grains are dislocation free, and lower the bulk energy density of the parent grain. The strain energy $\mathcal{E}_m^v$ of a crystal of phase m is then given by the volume average between the relict part of the grain, with a density of dislocation ρ, and the dislocation-free nucleated part of the grain,

$$\mathcal{E}_m^v = \alpha A\rho\mu b^2, \tag{6}$$

where α is the volume fraction of the crystal occupied by the relict non-recrystallized part of the grain. In Kaminski & Ribe (2001) the volume fraction of the relict part of the grain is given as a function of the square of the strain energy, i.e. of the square of the density of dislocation,

$$\alpha = \exp\left(-\lambda_m \rho^2\right) \equiv \exp\left[-\lambda_m^* \left(\frac{\rho}{\rho_o}\right)^2\right], \tag{7}$$

with λ_m a nucleation parameter related to the efficiency of nucleation (the larger λ_m, the larger the nucleation rate) which may be a function of the applied stress, of the temperature and/or of the amount of water. A dimensionless nucleation parameter is introduced,

$$\lambda_m^* = \lambda_m \rho_o^2, \tag{8}$$

with ρ_o the reference dislocation density obtained from the strain rate scale using Orowan's equation,

$$\dot{\epsilon}_o = \rho_o b v, \tag{9}$$

with v the velocity of dislocations and $\dot{\epsilon}_o$ the strain rate scale, defined by the maximum absolute value of the eigenvalues of the external strain rate tensor.

To estimate the strain energy of a crystal, it is thus sufficient to know its density of dislocations. At steady state, the density of dislocation is proportional to stress to the power $p \approx 1.5$ (Durham *et al.* 1977; Poirier 1985; Bai & Kohlstedt 1992). As the strain rate is itself proportional to the stress to the power n, the density of dislocation is proportional to the strain rate to the power p/n. The resulting expression for the dimensionless strain energy of the grain is then

$$E_m^v = \frac{\mathcal{E}_m^v}{A\rho_o\mu b^2} = \sum_s I_v^{s^*} \exp\left[-\lambda_m^* \left(I_v^{s^*}\right)^2\right], \tag{10}$$

where

$$I_v^{s^*} = \left(\frac{\tau_o}{\tau_m^s}\right)^{n-p} \left|\frac{\dot{\epsilon}_v^s}{\dot{\epsilon}_o}\right|^{p/n}, \tag{11}$$

with $\dot{\epsilon}_v^s \equiv \beta_m^{sv}\gamma^v$ the strain rate on the slip system s. These relationships would break down if the density of dislocations cannot be considered to be in steady state, i.e. for strains smaller than 1 per cent. In consequence the model should not apply to the case of static recrystallization.

Once the strain rate scale $\dot{\epsilon}_o$ has been calculated from the externally imposed velocity gradient tensor D_{ij}, the dimensionless strain energy of the grains is obtained from the strain energy equations (10) and (11). The strain energy is then a function only of the dimensionless reference resolved shear stress of the shear planes of the different mineral phases, and of the value of the dimensionless nucleation rate λ_m^*. The values of the RRSS are given in Table 1 for enstatite and olivine. The value of λ_m^* has been estimated by Kaminski & Ribe (2001) to be about 5 from comparison with LPO obtained in experimental deformations of olivine aggregates. No experiments are yet available to estimate the value of λ_m^* for enstatite. For now we will use the same value for enstatite as for olivine.

3.3 Grain-boundary migration

Given the strain energy densities of all grains in the aggregate, the change of the volume fraction f_m^v of a grain of a phase m due to dynamic recrystallization is given by the dimensionless equation

$$\frac{df_m^v}{dt^*} = -M_m^* f_m^v \left(E_m^v - \bar{E}_m\right), \tag{12}$$

where $t^* = \dot{\epsilon}_o t$ is the dimensionless time and $\bar{E}_m$ is the dimensionless volume average strain energy for phase m,

$$\bar{E}_m = \sum_v f_m^v E_m^v. \tag{13}$$

As in the calculation of the plastic deformation of the crystals, we assume here that each crystal is subject to the same mean energy. Eq. (12) contains in addition a dimensionless grain-boundary mobility

$$M_m^* = X_m \frac{A\mu b M_m}{v}, \tag{14}$$

with M_m the 'intrinsic' grain-boundary mobility, and X_m the volume fraction of phase m in the aggregate. The volume fraction X_m implies here that grain-boundary migration is 'geometrically' less efficient in a multiphase aggregate because only that portion of the surface of a grain that is in contact with minerals of the same phase may migrate. For an aggregate of 100 per cent olivine, comparison with experimental data yields $M_{ol}^* = 125 \pm 75$. Here again, as no information is available for enstatite yet, we will use the same value for the two phases.

3.4 Grain-boundary sliding

We assume that grain-boundary sliding is the dominant mechanism of deformation for small grains. A grain deforms dominantly by grain-boundary sliding if its volume is smaller than a threshold volume. Because the present model is based on volume fractions and does not specify explicitly the size of the grains, we express the activation of grain-boundary sliding in term of volume fractions as

$$\frac{f^v}{f_{gbs}} \leq 1, \tag{15}$$

where f_{gbs} is the threshold volume fraction for the activation of grain-boundary sliding. Multiplied by the total volume of the aggregate, f_{gbs} gives the threshold volume. Because volume fractions are usually small numbers which are difficult to interpret, we will use in the following the ratio of f_{gbs} over the initial volume fraction f_o of each grain,

$$\chi \equiv \frac{f_{gbs}}{f_o}. \tag{16}$$

The threshold 'dimensionless' volume fraction χ is the third free parameter of the model. When the volume fraction of a grain decreases to χf_o, the grain deforms by grain-boundary sliding instead of dislocation creep. As a consequence it does not rotate by plastic deformation anymore, and its strain energy is set to zero. Such a threshold can be interpreted as the minimum dislocation length necessary to emit dislocations (Poirier 1985). This ensures a vanishing density of dislocations in very small grains even at large stress. If χ is close to 0, then the fraction of grains deformed dominantly by grain-boundary sliding is negligible and the model is equivalent to Kaminski & Ribe (2001). If χ is larger than 1, all the grains deform by grain-boundary sliding and the distribution of orientations stays uniform. The actual value of χ is between 0 and 1 and can be constrained by comparison with experiments.

A major point of interest of the experiments of Bystricky *et al.* (2000) is that they give the evolution of the total LPO, i.e. not only of the large relict grains but also of the small grains generated by dynamic recrystallization. These small grains are precisely the ones supposed to affected by grain-boundary sliding (Lee *et al.* 2002). The comparison between the data of Bystricky *et al.* (2000) (complete LPO) and Zhang *et al.* (2000) (mainly relict grains) shows one common point and one difference. The common point of the two sets of experiments is the early development of a main peak aligned with the shear direction. The location and the rate of growth of this peak have been used to estimate λ^* and M^* in Kaminski & Ribe (2001). Furthermore, in the two sets of experiments a secondary peak is also present 45° away from the main peak. This peak is formed by grains in a hard orientation characterized by a small density of dislocations. Their strain energy is only slightly larger than that of the recrystallized soft grains so their rate of shrinking is small. The difference between the two sets of experiments is that in Zhang *et al.* (2000) the relict grains forming that peak eventually disappear at about 100 per cent strain whereas in Bystricky *et al.* (2000) the secondary peak is still present at 500 per cent strain. It is likely that this peak is formed by small grains measured only in Bystricky *et al.* (2000).

If one knows both the orientation Φ_{II} of the secondary peak (i.e. 45° away from the shear direction) and the orientation Φ_I of the main peak (i.e. the shear direction) in the [100] plane, the average orientation can be estimated as

$$\Phi_a = (1 - r)\Phi_{II} + r\Phi_I, \tag{17}$$

where r is the volume fraction of the main peak. This estimation is accurate at strains larger than 50 per cent as the two main peaks did not dominate the LPO before. We estimated r from Fig. 4 of Bystricky *et al.* (2000) by weighting the volume of the main and the secondary peak, and we compared it with the value obtained for various value of χ in the model. Fig. 1 gives the prediction of the model for 100 per cent strain in simple shear for two values of χ. If $\chi = 0$, the secondary peak is small and vanishing as in Zhang & Karato (1995), whereas for $\chi = 0.4$ the secondary peak is about twice as intense, closer to the results of Bystricky *et al.* (2000). Fig. 2 shows the result of the calculations for $M_{ol}^* = 125$: the experimental data require a threshold dimensionless volume χ of 0.3 ± 0.1. For values of χ smaller than 0.2, the secondary peak disappears too early whereas for values of χ larger than 0.4, the secondary peak is too strong.

We made additional calculations to test the influence of the grain-boundary mobility on the value of χ. We found that for a given value of χ, the evolution of the strength of the secondary peak depends only weakly on the inferred value of M_{ol}^*. This is due to the interaction between grain-boundary migration and the weakening of the LPO by grain-boundary sliding of small grains. For example, if the grain-boundary mobility is large, the main peaks grows faster and 'sharpens' the LPO. However, the fraction of small grains increases faster and grain-boundary sliding will be more active, 'softening' the LPO and cancelling the previous effect.

4 IMPLICATIONS OF THE MODEL

Our previous studies focused on the LPO evolution induced by dynamic recrystallization of an olivine polycrystal with no grain-boundary sliding (Kaminski & Ribe 2001, 2002; Kaminski 2002).

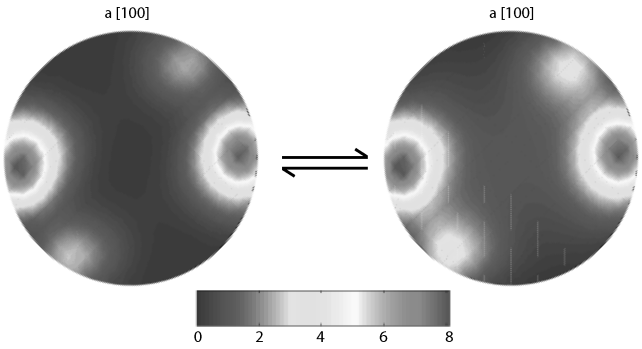

Figure 1. Pole figures (Lambert equal-area projection; the grey scale corresponds to the density of the orientation distribution function expressed as multiples of a uniform distribution) predicted by the model for the [100] (*a*) axis for two values of χ (left $\chi = 0$, right $\chi = 0.4$) and 100 per cent strain for a dextral simple shear. The strength of the secondary peak 45° away from the shear direction increases with χ.

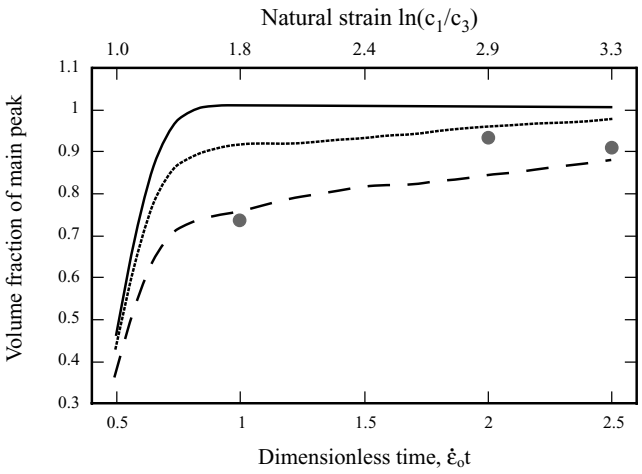

Figure 2. Evolution of the surface fraction of the pole figure occupied by the main peak in the shear plane for $\chi = 0$ (solid line), 0.2 (dotted line) and 0.4 (dashed line.) The circles are estimates from the laboratory experiments of Bystricky *et al.* (2000).

The main results of these studies were the following. For an efficient nucleation process ($\lambda^* \geq 3$) grain-boundary migration favours grains in soft orientations, in which the deformation on the softest slip system is maximum. In the case of a homogeneous deformation, these grains then rotate plastically as a function of strain towards a steady-state orientation. This steady state, in dry conditions, is such that the *a*-axis of the grains is aligned with the long axis of the finite strain ellipsoid in the limit of an infinite strain, or infinite strain axis (ISA) (see Appendix B). In simple shear the ISA is simply the shear direction. In water-rich conditions, the steady state is such that the *c*-axis of the grains is aligned with the ISA. The time required to reach the steady state is $\tau_{\rm ISA} \approx 3/\dot{\epsilon}_{\rm o}$. These results are affected by the refinements introduced in the new formulation of the model.

4.1 Incorporation of enstatite

Fig. 3 shows the prediction of the model for an aggregate of 70 per cent olivine and 30 per cent enstatite and 4394 grains, for a simple shear deformation to 100 per cent strain ($\dot{\epsilon}_{\rm o} t = 0.5$). Because there is no interaction between olivine and enstatite, the olivine LPO is almost the same with or without enstatite (see Fig. 2 of Kaminski & Ribe 2001), only a bit less concentrated, as the effective grain-boundary mobility is decreased in the two-phase aggregate (eq. 14). The figure also confirms a well-known result of purely plastic deformation models (Ribe 1992; Blackman *et al.* 2002): enstatite crystals align perpendicularly with the olivine crystals (the *a*-axis of olivine is aligned with the *c*-axis of enstatite and the *c*-axis of olivine is aligned with the *b*-axis of enstatite). One may note also that the enstatite LPO is less concentrated than the olivine LPO. Because only one slip system is active in enstatite, the density of dislocations is smaller than in olivine and there is less strain energy to drive dynamic recrystallization. Furthermore, the volume fraction of enstatite and thus its effective grain-boundary mobility are smaller than those for olivine. With or without dynamic recrystallization, the effect of enstatite is a net decrease of the total anisotropy.

4.2 Grain-boundary sliding

The first consequence of grain-boundary sliding is to keep the number of grains constant for any value of χ larger than zero. When a grain becomes smaller than the threshold volume, it does not deform plastically and its strain energy decreases to zero. This grain will then tend to grow by grain-boundary migration and will never shrink and disappear. Taking into account grain-boundary sliding of small grains thereby prevents the LPO from becoming singular even at large strains. However, because $\chi \ll 1$, grain-boundary sliding involves only a small volume fraction of the aggregate and is never the dominant deformation mechanism.

The second consequence of grain-boundary sliding is a change in the evolution of the average orientation of the aggregate at large strain. Fig. 4 shows the evolution of the orientation of the average *a*-axis in the aggregate with and without grain-boundary sliding for simple shear. At the beginning of the deformation the evolutions are similar. At large strains, however, the rotation of the average orientation to the shear plane is more sluggish when grain-boundary sliding is active. We have seen that grain-boundary sliding induces a secondary peak 45° away from the main peak. This shifts the average orientation of the aggregate from the main peak towards the secondary peak orientation and slows down the bulk rotation of the aggregate towards the shear direction. In all the cases the average orientation will align with the shear direction for sufficiently large strains. However, the time required to reach the steady-state orientation is larger with grain-boundary sliding, by about a factor 3 for $\chi = 0.2$ and about a factor 5 for $\chi = 0.4$.

The effect of grain-boundary sliding is more complex when the deformation changes as a function of time. To study that point, we consider a plane strain deformation evolving from a pure shear to a simple shear in a dimensionless time $5\dot{\epsilon}_{\rm o} t$. A plane strain deformation is defined by only two non-zero rates of strain $E_{11} = -E_{22} = \dot{\epsilon}_{\rm o}$, and by a variable rotational component of magnitude $|\Omega|$ about the x_3-axis. $|\Omega|$ defines a dimensionless 'vorticity number' $\Gamma = \Omega/\dot{\epsilon}$. Pure shear corresponds to $\Gamma = 0$ and simple shear to $\Gamma = \pm 1$. In the present calculation, the vorticity number Γ is

$$\Gamma = \frac{1}{5}\dot{\epsilon}_{\rm o} t, \tag{18}$$

which for a dimensionless time between 0 and 5 corresponds to a deformation evolving from a pure shear to a simple shear (see Fig. 4 of Kaminski & Ribe 2002, for a graphical illustration of the streamlines of the corresponding flows). Fig. 5 shows the evolution of the mean orientation of the *a*-axis in the plane of deformation and the orientation of the infinite strain axis ($\Phi_{\rm ISA} = 0.5 \sin^{-1} \Gamma$). When

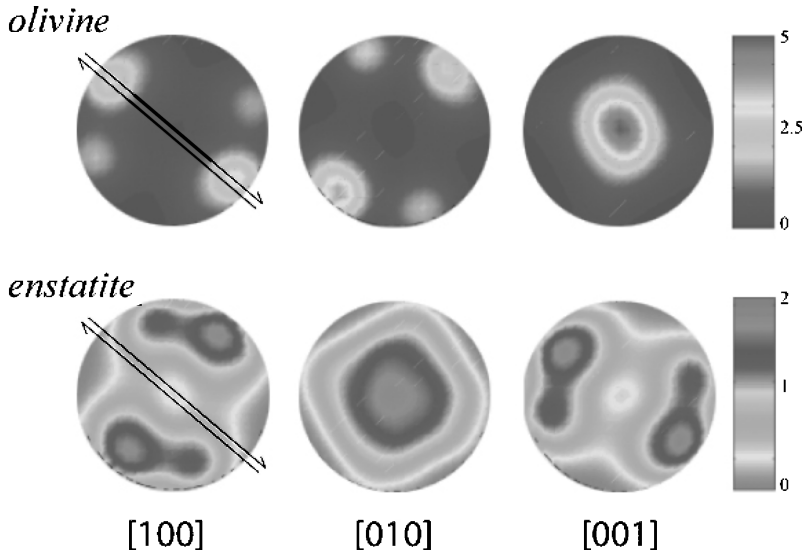

Figure 3. Pole figures for the [100], [010] and [001] crystallographic axes for an aggregate comprising 70 per cent olivine and 30 per cent enstatite deformed by dextral simple shear to 100 per cent strain ($\dot{\epsilon}t = 0.5$). Parameters for dynamic recrystallization are $\lambda^* = 5$ and $M^* = 125$ for both olivine and enstatite.

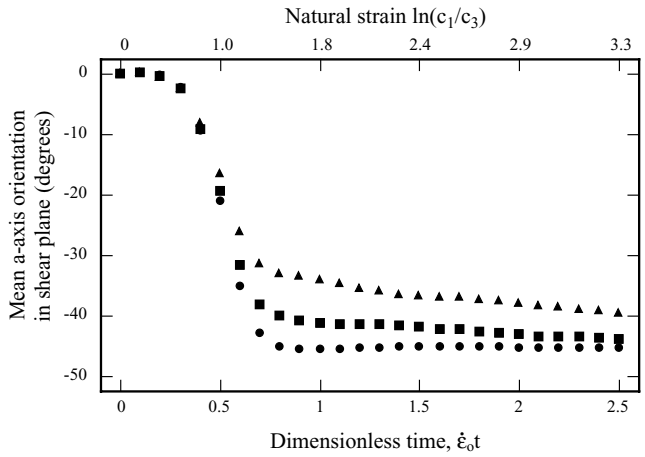

Figure 4. Evolution of the average *a*-axis orientation in simple shear as a function of strain for a pure olivine aggregate and $\chi = 0$ (circles), 0.2 (squares) and 0.4 (triangles.)

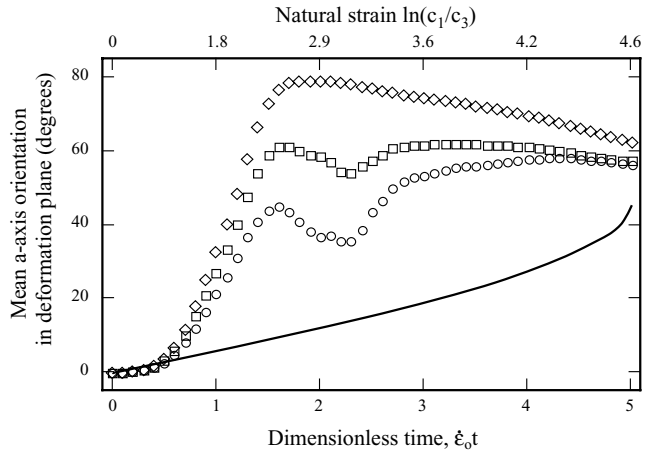

Figure 5. Evolution of the average *a*-axis orientation for a planar deformation that evolves from pure shear to simple shear over a dimensionless time $\dot{\epsilon}_o t = 5$. Results are shown for $\chi = 0$ (diamonds), 0.2 (squares) and 0.4 (circles). The infinite strain axis orientation is given by the solid curve.

grain-boundary sliding is present, the LPO rotates faster towards the direction of the infinite strain axis. This is due to the presence of secondary peaks nourished by boundary sliding of small grains generated by grain-boundary migration (as in the simple shear example). Because a small grain whose orientation lies in a secondary peak deforms by grain-boundary sliding, its strain energy is zero and it will grow by grain-boundary migration. Grain-boundary sliding then becomes inactive and the grain again starts to deform plastically and will eventually rotate to a new orientation. As a function of the energy associated with its new orientation the grain can grow or shrink, which makes the evolution of the average orientation oscillate. Moreover, if the new orientation of the grain is aligned with the ISA, the grain will by definition keep this steady-state orientation. This in turn increases the bulk rotation rate of the aggregate towards the ISA.

Kaminski & Ribe (2002) showed that olivine LPO in the mantle will follow the convective flow direction only if the time required for the crystals to reach a steady-state LPO is smaller than the timescale over which the deformation varies along a pathline. This condition is quantified by the introduction of a dimensionless number, the grain orientation lag (GOL) parameter, defined by the ratio of the two times. This parameter has to be much smaller than 1 for the LPO to follow the flow direction. The precise threshold value of this parameter for the *a*-axis orientation to be aligned with the flow direction is difficult to give. It depends on the exact value of the grain-boundary mobility, on the nature of the deformation (Kaminski & Ribe 2002) and on the value of the threshold activation volume of grain-boundary sliding. A rule of thumb based on diverse numerical experiments we have performed is that the GOL parameter must be smaller than 0.5 for the LPO to be aligned with the flow direction within 5°.

4.3 A complete example

To illustrate how one can use D-Rex to study the anisotropic signature of a convective flow, we take the example of a simple analytical corner flow. This flow has been used previously in Kaminski & Ribe (2002) to illustrate the relationship between the LPO and the flow direction. Here we illustrate the kind of seismic information provided by the complete model.

Let U be the half spreading rate, and let (r, θ) be polar coordinates with origin at the ridge axis such that $\theta = 0$ is vertical. The equations of slow viscous flow admit a similarity solution in which the velocity $\vec{u}$ is a function of θ only (Batchelor 1967, p. 224):

$$\vec{u} \cdot \hat{r} = \frac{2U}{\pi}(\theta \sin\theta - \cos\theta), \quad \vec{u} \cdot \hat{\theta} = \frac{2U}{\pi}\theta\cos\theta. \tag{19}$$

To apply this model to the Earth, we suppose that $\theta = \pi/2$ corresponds to the Earth's surface while $z = r\cos\theta = 1$ is the depth of the phase change α-olivine to β-spinel. We suppose that the aggregates are isotropic at that depth, and follow the evolution of the LPO along pathlines. The LPO evolves by plastic deformation and dynamic recrystallization with $M^* = 125$, $\lambda^* = 5$ and $\chi = 0$ or 0.4.

The raw product of D-Rex is the orientation distribution function of the crystals forming the aggregate, i.e. their volume fractions and orientations. Knowing the seismic properties of olivine and enstatite crystals, one can calculate the global elastic tensor for the aggregate by Voigt averaging (Mainprice 1990). We calculate in D-Rex the best hexagonal approximation of the resulting tensor using a projection method described in detail in Browaeys & Chevrot (2003). Hexagonal symmetry is the usual approximation used in seismic studies and gives the best readability to the model outputs.

Fig. 6 shows the orientation of the fast axis of the hexagonal tensor and the percentage of anisotropy for two cases: a pure olivine aggregate without grain-boundary sliding and an aggregate including 30 per cent enstatite and a threshold volume for grain-boundary sliding $\chi = 0.4$. The predictions of orientations are similar, because in the two cases the dominant orientation in the aggregate is the main peak of olivine. Inclusion of enstatite and grain-boundary sliding changes the predicted anisotropy in two significant ways. First, the total anisotropy is reduced, which yields a more common value of 8 per cent of anisotropy for the flow. Second, a 'quasi-single-crystal' instability far from the ridge (the fast axis rotates away from the flow direction) is suppressed.

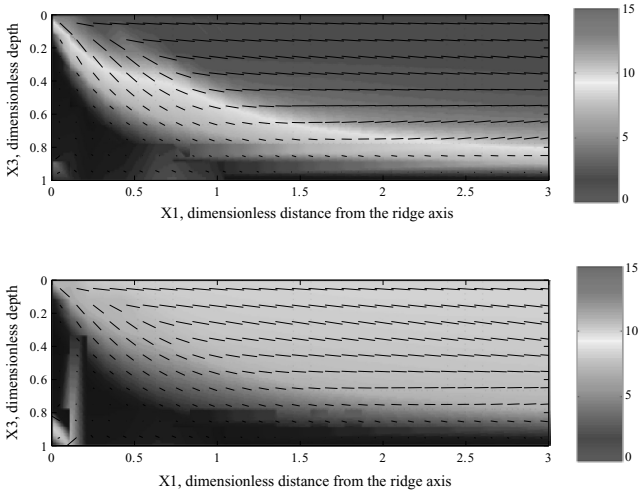

Figure 6. Orientation of the axis of fast propagation (bars) and percentage of anisotropy (grey scale) for an aggregate in the corner flow defined by eq. (19). The anisotropy shown is that of the medium with hexagonal symmetry that best fits the full elastic tensor predicted by D-Rex. Upper diagram: prediction without grain-boundary sliding ($\chi = 0$) and without enstatite. Lower diagram: prediction with 30 per cent enstatite and $\chi = 0.4$. The strong anisotropy in the lower left corner shows that the hexagonal approximation is not correct in that region.

5 DISCUSSION

Many theoretical points concerning dynamic recrystallization are still subject to debate and our model is no exception. However, it is based on well-established physical mechanisms and provides a real quantitative test of its underlying hypotheses. In particular, the value of the free parameters (nucleation parameter λ^*, grain-boundary mobility M^* and threshold volume for the activation of grain-boundary sliding χ) is constrained by comparison with laboratory experiments. Additional ingredients—like a randomization due to subgrain rotation or an explicitly random rotation of the crystals associated with grain boundary sliding—might be added to the model, but are not required by the present set of experimental constraints. The precise value of the physical parameters is hidden in the dimensionless parameters M^*, λ^* and χ. For example, the real value of the velocity of the dislocations or the threshold size for activation of grain-boundary sliding are not given. The aim of the model, however, is not to predict detailed microstructures as a numerical equivalent of laboratory experiments. Because that requires a treatment of each process at the level of the dislocations and an exact calculation of the evolution of each grain in the aggregate, it also requires much larger computational resources and complex mathematical and numerical techniques (Jessell *et al.* 2001). The model nevertheless encompasses the basic physics of dynamic recrystallization in a simple first-order theory. Due to the simplifications it uses, the model has a semi-analytical solution and is very fast and easy to implement in conjunction with 3-D numerical convective codes. It can be used to build the missing link between microstructure observations in the laboratory, numerical calculation of convective flows and synthetic seismograms, and measurements of seismic anisotropy in the field.

The biggest restriction of our model, shared by all others, is that it is based only on parametrized laboratory experiments performed at relatively high strain rates and stresses relative to real Earth conditions. The extrapolation of laboratory predictions to natural situations has been a long-standing problem in microstructural studies. However, when the deformation history of the natural samples is known, especially in a shear zone, one can conduct a precise comparison between microstructural field observations and laboratory and theoretical results. In such cases, Hirth (2004) has recently been able to show that the evolution of the LPO obtained in the laboratory by Zhang & Karato (1995) was close to the evolution observed in naturally deformed rocks. In particular, the rotation rate of the mean a-axis towards the shear direction as a function of increasing strain is similar in the two cases. The values of the parameters we have constrained from various laboratory experiments may thus be appropriate for actual Earth conditions.

6 CONCLUSION

The model described in this paper includes randomization by grain-boundary sliding of small grains in order to obtain more realistic LPO at large strains. It includes three free parameters, the threshold dimensionless volume for activation of grain-boundary sliding χ, the nucleation parameter λ^* and the grain-boundary mobility M^* which have been constrained by comparison with laboratory experiments (Table 2). As a function of these parameters and of a prescribed history of deformation, the model predicts the LPO evolution of an aggregate of $X_{\rm ol}$ per cent of olivine and $100-X_{\rm ol}$ per cent of enstatite (see Appendix A). The LPO predicted by the model does not become singular and the calculation is much more

Table 2. Free parameters of the model.

Parameter	Range of value	Experimental constraints
λ^*	≈ 5	Evolution of main orientation and of J index + LPO snapshots (Zhang & Karato 1995; Zhang *et al.* 2000; Nicolas *et al.* 1973)
M^*	125 ± 75	Evolution of main orientation and of J index + LPO snapshots (Zhang & Karato 1995; Zhang *et al.* 2000; Nicolas *et al.* 1973)
χ	0.3 ± 0.1	Evolution of the strength of secondary peak orientation at large strains (Bystricky *et al.* 2000)

stable and robust than in the former version of the model. The incorporation of enstatite, which tends to align perpendicularly with olivine, decreases the net anisotropy which will yield smaller and thus more realistic percentages of anisotropy. A Fortran 90 code for this model, called D-Rex, can be found on our web site at http://www.ipgp.jussieu.fr/∼kaminski.

ACKNOWLEDGMENTS

We thank Andrea Tommasi and Harro Schmeling for their constructive review. We acknowledge fruitful interactions and discussions with Andrea Tommasi, Greg Hirth, Shun-Ichiro Karato, Mark Jessel and Jean-Paul Poirier during our studies on dynamic recrystallization. Sébastien Chevrot suggested the analytical solution in Appendix B.

REFERENCES

Bai, Q. & Kohlstedt, D.L., 1992. High-temperature creep of olivine single crystals. 2. Dislocation structures, *Tectonophysics,* **206,** 1–29.

Bai, Q., Mackwell, S.J. & Kohlstedt, D.L., 1991. High-temperature creep of olivine single crystals. 1. Mechanical results for buffered samples, *J. geophys. Res.,* **96,** 2441–2463.

Batchelor, G.K., 1967. *An Introduction to Fluid Dynamics,* Cambridge University Press, London.

Becker, T.W., Kellogg, J.B., Ekström, G. & O'Connell, R.J., 2003. Comparison of azimuthal seismic anisotropy from surface waves and finite-strain from global mantle-circulation models, *Geophys. J. Int.,* **155,** 696–714.

Blackman, D.K., Wenk, H.-R. & Kendall, J.-M., 2002. Seismic anisotropy of the upper mantle: 1. Factors that affect mineral texture and effective elastic properties, *Geochem. Geophys. Geosyst.,* **9,** doi:10.129/2001GC000248.

Browaeys, J.T. & Chevrot, S., 2003. Decomposition of the elastic tensor and geophysical applications. *Geophys. J. Int.,* in press.

Bystricky, M., Kunze, K., Burlini, L. & Burg, J.-P., 2000. High shear strain of olivine aggregates: rheological and seismic consequences, *Science,* **290,** 1564–1567.

Chastel, Y.B., Dawson, P.R., Wenk, H.R. & Bennet, K., 1993. Anisotropic convection with implications for the upper mantle, *J. geophys. Res.,* **98,** 17 757–17 771.

Dawson, P.R. & Wenk, H.-R., 2000. Texturing of the upper mantle during convection, *Phil. Mag. A,* **80,** 573–598.

Dick, H. J.B., Fisher, R.L. & Bryan, W.B., 1984. Mineralogic variability of the uppermost mantle along mid-oceanic ridges, *Earth planet. Sci. Lett.,* **69,** 88–106.

Durham, W.B. & Goetze, C., 1977. Plastic flow of oriented single crystals of olivine. 1. Mechanical data, *J. geophys. Res.,* **82,** 5737–5753.

Durham, W.B., Goetze, C. & Blake, B., 1977. Plastic flow of oriented single crystals of olivine. 2. Observations and interpretations of the dislocation structure, *J. geophys. Res.,* **82,** 5755–5770.

Etchecopar, A., 1977. A plane kinematic model of progressive deformation in a polycrystalline aggregate, *Tectonophysics,* **39,** 121–139.

Gantmacher, F.R., 1989. *The Theory of Matrices,* vol. 2, Chelsea Publishing Company, New York.

Hanson, D.R. & Spetzler, H.A., 1994. Transient creep in natural and synthetic, iron-bearing olivine single crystals: mechanical results and dislocation microstructure, *Tectonophysics,* **235,** 293–315.

Hildebrand, F.B., 1952. *Methods of Applied Mathematics,* Prentice-Hall, Englewood Cliffs, NJ.

Hirth, G., 2004. Lattice preferred orientations in naturally deformed peridotites: a link from the lab to mantle dynamics, *EOS, Trans. Am. Geophys. Un.,* **84**(46, Supplement), F1209.

Jessell, M., Bons, P., Evans, L., Barr, T. & Stüwe, K., 2001. Elle: the numerical simulation of metamorphic and deformation microstructures, *Comput. Geosci.,* **27,** 7–30.

Jin, Z.M., Bai, Q. & Kholdstedt, D.L., 1994. High temperature creep of olivine crystals from four localities, *Phys. Earth planet. Int.,* **82,** 55–64.

Jung, H. & Karato, S.I., 2001. Water-induced fabric transitions in olivine, *Science,* **293,** 1460–1463.

Kaminski, E., 2002. The influence of water on the development of lattice preferred orientation in olivine aggregates, *Geophys. Res. Lett.,* **12,** 17-1–17-4.

Kaminski, E. & Ribe, N.M., 2001. A kinematic model for recrystallization and texture development in olivine polycrystals, *Earth planet. Sci. Lett.,* **189,** 253–267.

Kaminski, E. & Ribe, N.M., 2002. Time scales for the evolution of seismic anisotropy in mantle flow, *Geochem. Geophys. Geosyst.,* **8,** 1–17.

Karato, S.I., 1987. Seismic anisotropy due to lattice preferred orientation of minerals: kinematic or dynamic, in *High-Pressure Research in Mineral Physics,* pp. 455–471, eds Manghani, M.H. & Syono, Y., American Geophysical Union, Washington, DC.

Karato, S.-I., Paterson, M.S. & Gerald, J.D.F., 1986. Rheology of synthetic olivine aggregates: influence of grain size and water, *J. geophys. Res.,* **91,** 8151–8176.

Kohlstedt, D.L. & Goetze, C., 1974. Low-stress high-temperature creep in olivine single crystals, *J. geophys. Res.,* **79,** 2045–2051.

Lee, K.-H., Jiang, Z. & Karato, S.-H., 2002. A scanning electron microscope study of the effects of dynamic recrystallization on lattice preferred orientation in olivine, *Tectonophysics,* **351,** 331–341.

Mainprice, D., 1990. A Fortran program to calculate seismic anisotropy from the lattice preferred orientation of minerals, *Comput. Geosci.,* **16**(3), 385–393.

McKenzie, D.P. & Jackson, J., 1983. The relation between strain rates, crustal thickening, paleomagnetism, finite strain and fault movements within a deforming zone, *Earth planet. Sci. Lett.,* **65,** 182–202.

Nicolas, A. & Christensen, N.I., 1987. Formation of anisotropy in upper mantle peridotites: a review, in *Composition, Structure and Dynamics of the Lithosphere–Asthenosphere System,* American Geophysical Union Geodynamics Monograph Series, pp. 111–123, eds Fuchs, K. & Froidevaux, C., American Geophysical Union, Washington, DC.

Nicolas, A., Boudier, F. & Boullier, A.M., 1973. Mechanisms of flow in naturally and experimentally deformed peridotites, *Am. J. Sci.,* **273,** 853–876.

Poirier, J.-P., 1985. *Creep of Crystals,* Cambridge University Press, Cambridge.

Poirier, J.-P. & Guillopé, M., 1979. Deformation induced recrystallization of minerals, *Bull. Mineral.,* **102,** 67–74.

Raleigh, C.B.S., Kirby, S.H., Carter, N.L. & AveLallemant, H.G., 1971. Slip and the clinoenstatite transformation as competing rate process in enstatite, *J. geophys. Res.,* **76,** 4011–4022.

Ribe, N.M., 1992. On the relation between seismic anisotropy and finite strain, *J. geophys. Res.,* **97,** 8737–8747.

Ribe, N.M. & Yu, Y., 1991. A theory for plastic deformation and textural evolution of olivine polycrystals, *J. geophys. Res.,* **96,** 8325–8335.

Takeshita, T., Wenk, H.R., Canova, G.R. & Molinari, A., 1990. Simulation of dislocation assisted plastic deformation in olivine polycrystals, in *Deformation Mechanisms in Minerals and Ceramics,* pp. 365–376, eds Barber, D.J. & Meredith, P.G., Allen and Unwin, London.

Tommasi, A., 1998. Forward modeling of the development of seismic anisotropy in the upper mantle, *Earth planet. Sci. Lett.,* **160,** 1–18.

Tommasi, A., Mainprice, D., Canova, G. & Chastel, Y., 2000. Viscoplastic self-consistent and equilibrium-based modelling of olivine lattice preferred orientations. 1. Implications for the upper mantle seismic anisotropy, *J. geophys. Res.,* **105,** 7893–7908.

Weidner, D.J., Wang, H. & Ito, J., 1978. Elasticity of orthoenstatite, *Phys. Earth planet. Int.,* **17,** 1–13.

Wenk, H.R. & Tomé, C.N., 1999. Modeling dynamic recrystallization of olivine aggregates deformed in simple shear, *J. geophys. Res.,* **104,** 25 513–25 527.

Wenk, H.R., Bennett, K., Canova, G. & Molinari, A., 1991. Modelling plastic deformation of peridotite with the self-consistent theory, *J. geophys. Res.,* **96,** 8337–8349.

Zhang, S. & Karato, S.I., 1995. Lattice preferred orientation of olivine aggregates deformed in simple shear, *Nature,* **375,** 774–777.

Zhang, S., Karato, S.I., Gerald, J.F., Faul, U.H. & Zhou, Y., 2000. Simple shear deformation of olivine aggregates, *Tectonophysics,* **316,** 133–152.

APPENDIX A: INPUTS AND OUTPUT OF D-REX

D-Rex is a Fortran 90 code that can be used to calculate the LPO evolution of an aggregate of olivine and enstatite in arbitrary proportions. For each deformation step the code requires the following inputs:

(0) A former orientation distribution function (random in the reference version of the code).

(1) The externally imposed velocity gradient tensor $D_{ij} = \partial v_i/\partial x_j$.

(2) The activity of the slip systems of olivine and enstatite (e.g. Table 1), which may depend on the amount of water.

(3) The value of the grain-boundary mobility M^*.

(4) The value of the threshold dimensionless volume for grain-boundary sliding χ.

The output of the code is the time derivative of the orientation distribution of the aggregate (i.e. orientation and volume of the crystals). The code can be used as a subroutine to integrate the changes of the orientation distribution function along a pathline. From the resulting LPO, an elastic tensor can be calculated by Voigt or Reuss averaging. A transverse isotropic approximation of the elastic tensor can also be calculated.

APPENDIX B: ANALYTICAL CALCULATION OF THE INFINITE STRAIN AXIS ORIENTATION

The orientation of the 'infinite strain axis' (ISA), when it exists, is given by the orientation of the long axis of the finite strain ellipsoid (FSE) in the limit of infinite strain. The FSE is obtained from the deformation gradient tensor $\boldsymbol{F}$, which satisfies

$$\frac{d\boldsymbol{F}}{dt} = \boldsymbol{L}\boldsymbol{F}, \tag{B1}$$

subject to the initial condition $\boldsymbol{F} = \boldsymbol{I}$, with $\boldsymbol{L}$ is the velocity gradient tensor and $\boldsymbol{I}$ the identity tensor. The solution of eq. (B1) is (Gantmacher 1989)

$$\boldsymbol{F} = \exp(\boldsymbol{L}t) = \boldsymbol{I} + \boldsymbol{L}t + \frac{\boldsymbol{L}^2}{2!}t^2 + \cdots . \tag{B2}$$

From $\boldsymbol{F}$, on can form a 'right stretch tensor' $\boldsymbol{U}$,

$$\boldsymbol{U} = \boldsymbol{F}^{\mathrm{T}}\boldsymbol{F}, \tag{B3}$$

with $\boldsymbol{F}^{\mathrm{T}}$ the transpose of $\boldsymbol{F}$. The eigenvectors of $\boldsymbol{U}$ give the direction of the axes of the FSE (McKenzie & Jackson 1983), and the ISA is the limit as $t \to \infty$ of the direction of the eigenvector corresponding to the largest eigenvalue.

To obtain the limit of $\boldsymbol{U}$ when $t \to \infty$, we first calculate the eigenvalues (real or imaginary) $\lambda_k (k = 1, 2, 3)$ of $\boldsymbol{L}$. The matrix $\boldsymbol{U}$ can then be rewritten using Sylvester's formula as (Hildebrand 1952)

$$\boldsymbol{F} = \sum_{k=1}^{3} \exp(\lambda_k t) \frac{\prod_{r\neq k}(\boldsymbol{L} - \lambda_r \boldsymbol{I})}{\prod_{r\neq k}(\lambda_k - \lambda_r)}. \tag{B4}$$

If λ_1 (say) has the largest norm and is real, then the ISA is the eigenvector corresponding to the largest eigenvalue of the auxiliary matrix $\boldsymbol{U}_{\mathrm{a}}$,

$$\boldsymbol{U}_{\mathrm{a}} = \left[\frac{\prod_{r\neq 1}(\boldsymbol{L} - \lambda_r \boldsymbol{I})}{\prod_{r\neq 1}(\lambda_1 - \lambda_r)}\right]^{\mathrm{T}} \left[\frac{\prod_{r\neq 1}(\boldsymbol{L} - \lambda_r \boldsymbol{I})}{\prod_{r\neq 1}(\lambda_1 - \lambda_r)}\right]. \tag{B5}$$

If one eigenvalue is equal to zero, then because the deformation is incompressible all the eigenvalues are zero and the deformation is a simple shear. The ISA orientation is then simply the flow direction. If only one eigenvalue is real, and its norm is smaller than the norm of the imaginary eigenvalues, the ISA is not defined.